INSTRUMENTATION FOR



PLASMA DIAGNOSTICS

by Harold P. Eubank

THE LAST DECADE has brought about enormous growth in efforts toward understanding plasmas. This growth has come primarily from two sources: the controlled-thermonuclear-research program and the space program, both of which have lent support to many research fields with overlapping interests, such as applied optics, low-energy-beam cross-section measurements and electromagnetic-wave propagation in ionized media.

Instrumentation for plasma diagnostics, a field concerned mainly with measurement of plasma temperatures and particle densities, is still in large part in the delightful stage of innovation and flux. Devices for plasma production, confinement and heating have provided considerable impetus for commercial development of very lowinductance, low-loss capacitors, reliable high-current switches, high-power vacuum tubes and energy-storage systems, as well as for improvement in ultrahigh vacuum technology. Similarly, the extremely short lifetimes that characterize some plasmas and the corresponding

rapid rate of change of plasma parameters have been largely responsible for development of the ultrafast photography now available in image-converter, rotating-prism and drum cameras with effective exposure times of about 10-s sec and framing rates of millions of exposures per second.

A number of books and article collections¹⁻⁶ have appeared during the last several years treating, in varying detail, almost every diagnostic method for obtaining plasma properties. We shall outline with comments the more familiar approaches, adding some remarks concerning a few techniques that have been discussed only lightly or not at all in the references above.

ELECTROMAGNETIC WAVES

The most admirably suited and versatile method for obtaining knowledge of plasmas is in their interaction with electromagnetic waves. Although plasmas can support a variety of waves with frequencies as low as the ionacoustic frequency,7 we concern ourselves here with the frequency range such that only electron motions are important. The effect of collisions could be incorporated into the treatment, but the tendency toward highertemperature plasmas with low neutral content and higher wave frequencies usually allows us to assume the simplification that the wave frequency is much greater than the momentum-transfer collision frequency.

Although the electron-density profile and the electron temperature can be

Efforts to measure plasma properties have been responsible for many instrumentation developments. Diagnostic methods now include a host of techniques used in other disciplines: interactions with electromagnetic waves, particle beams, probes, lasers and spectroscopy.



The author has been on the Princeton plasma physics laboratory staff since 1959. He studied at William and Mary, Syracuse, and Brown, where he received his doctorate. After five years as assistant

professor there, he went to Princeton.

inferred from probing with electromagnetic waves, the most common usage has been to measure the average electron density. For the resulting interaction, the plasma dispersion relation for a plane wave with frequency well above the value characterizing ion motion can be factored to yield solutions for two types of waves: (a) quasitransverse with electric-field vector perpendicular to wave vector and (b) quasi-longitudinal with electric-field vector parallel to wave vector. The transverse mode has, in turn, two values of index of refraction. The first is given by

$$\mu^{2} = \frac{1 - (\omega_{p}/\omega)^{2}}{1 - (\omega_{p}/\omega)^{2} \cos^{2} \theta}$$
 (1)

and defines the ordinary wave for which the plasma frequency is given by

$$\omega_{\rm p} = (n_{\rm e} e^2/\epsilon_0 m_{\rm e})^{\frac{1}{2}}$$

and θ is taken between the direction of the wave normal and the magnetic field. The second solution involves the electron cyclotron frequency and defines the extraordinary wave.

The wave in mode 1 obeys

$$\mu^2 = 1 - (\omega_p / \omega)^2$$
 (2)

when $\theta = \pi/2$ and is independent of the magnetic field for that direction. This mode of propagation is commonly employed for electron-density measurements, with the plasma and microwave horns inserted in one half of an interference bridge. When the plasma is inserted, the wave experiences a phase shift

$$\Delta \phi = \int_0^L (\mu_0 - \mu) \frac{2 \pi}{\lambda} dx$$

where μ_0 and μ are vacuum and plasma indices of refraction and L is the path length. This yields in terms of the electron density n_e ,

$$\Delta \phi = \int_0^L \left[1 - (1 - n_e/n_c)^{\frac{1}{2}}\right] \frac{2 \pi}{\lambda} dx$$
(3)

where n_c is termed the cutoff electron density for which $\omega_p = \omega$.

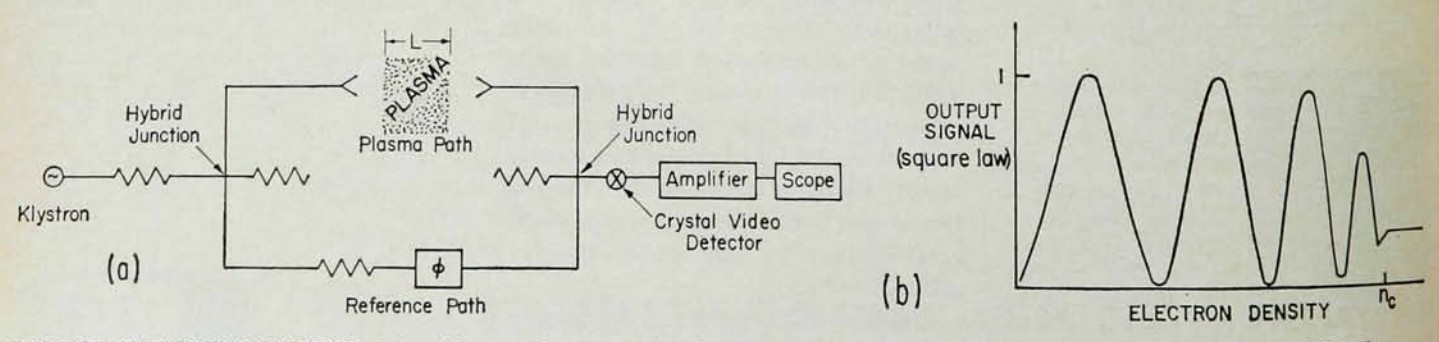
The nonlinear relationship between $\Delta \phi$ and n_e , which becomes pronounced when n_e approaches n_c , requires some knowledge of the plasma profile for accurate appraisal of the average electron density. M. A. Heald and C. B. Wharton³ discuss this problem in detail, pointing out the advantages of multiple-frequency and multiple-mode propagation.

In practice there are two conditions that set a lower limit on the frequency of the probing electromagnetic waves. The first is that ω exceed ω_p , and the second is the need to have the wavelength small compared to plasma dimensions so that the path through the plasma is the same over the dimensions of the beam. These two conditions usually require wave frequencies above 10 GHz, thus defining an electrondensity working range of $n_e \ge 10^{10}$ cm-3. The lower limit can, with care, be extended to about 10° cm-3 by klystron modulation and tuned-amplifier detection, but it must always be borne in mind when measuring phase shifts of 1 deg and less that even weak reflections from parts of the vacuum system, which will depend upon the presence of the plasma, can constitute a serious error as these reflected waves may have a large phase change.

A simple bridge interferometer is shown schematically in figure 1a. The response to a transient plasma appearing between the horns is illustrated by figure 1b, where both amplitude and phase effects are in evidence as n_e approaches n_e . If the bridge is initially balanced, maxima in the interference pattern correspond to multiples of 180-deg phase shifts.

A more sophisticated interferometer is the "fringe-shift" or "zebra-stripe" system of figure 2. Here amplitude effects are discriminated against with a balanced detector. One leg of the bridge is adjusted in length so that with frequency modulation of the klystron, differential phase changes occur in the two bridge legs to give a sinusoidal output from the detectors. These are then shaped and used for intensity modulation of the oscilloscope. Advantages of such fringe-shift interferometers are an oscilloscope deflection proportional to phase shift, continuous direct calibration and wide dynamic range. One disadvantage is the limitation set upon time resolution by the use of a sawtooth sweep frequency. Figure 3 illustrates the fringe display from a discharge in the Model C stellarator with a path length of 10 cm and a peak density of about 2.5 × 1011 cm⁻³.

For very low densities the cavity-perturbation method can be used if the cavity can be incorporated compatibly into the plasma vessel. S. C. Brown discusses several modes which can be used for low densities with and without magnetic field and for high densities where $\omega < \omega_p$. For $\omega \gg \omega_p$ and $\omega \gg \nu$ (ν is the collision frequency for momentum transfer) the TM₀₁₀ mode gives a frequency shift resulting from the presence of the plasma such that



BRIDGE INTERFEROMETER (a) with crystal output (b) shown as plasma density increases to cutoff value. -FIG. 1

$$\frac{\Delta \omega}{\omega} \approx \left(\frac{\omega_p}{\omega}\right)^2 \frac{1}{1 + \nu/\omega}$$
 (4)

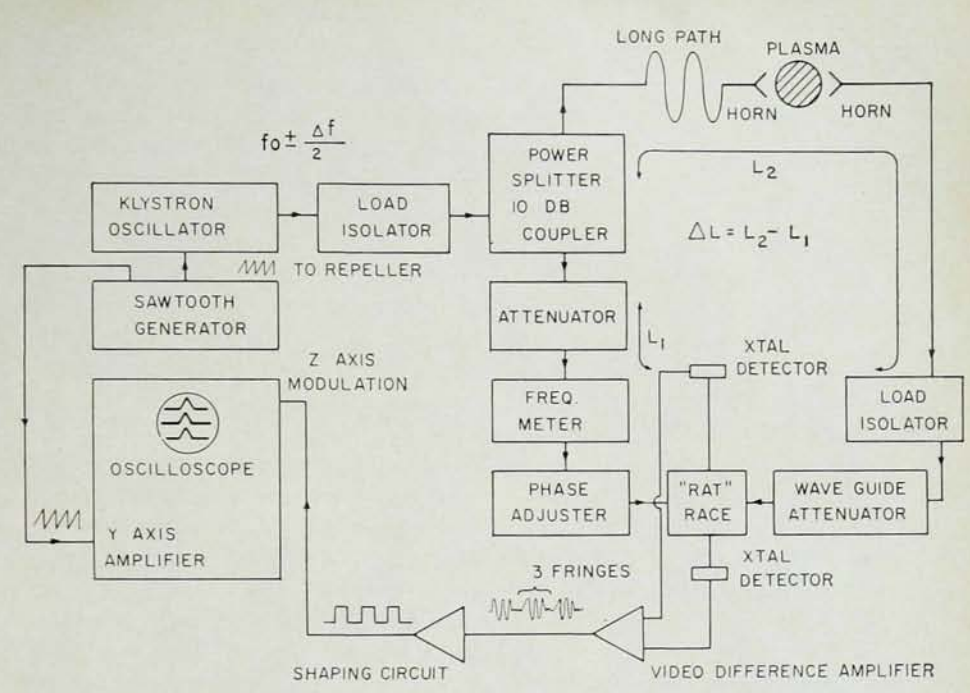
which can be used with or without an axial magnetic field since E is parallel to B.

Until the fairly recent discovery and development of coherent-radiation sources with wavelengths in the micron range, that is, the maser and laser, the electron density range above 10¹⁴ cm⁻³ was inaccessible to microwave transmission where the highest frequency commonly available in adequate power was about 100 GHz. The cutoff electron density giving a plasma frequency of 100 GHz is about 10¹⁴ cm⁻³. With monochromatic sources such as helium-neon lasers interferometric measurements of electron density have been extended to 10¹⁵–10¹⁸ cm⁻³.

The helium-neon laser has the desirable feature of emitting coupled radiation at wavelengths of 3.39 and 0.63 microns that originate from a common state. This laser has been used as its own resonator in which variation in the refractive index of the plasma produces modulation in the laser output. For a wavelength of 3.39 microns passing through 10 cm of plasma, a density of order 10¹⁶ cm⁻³ is required for a 90-deg phase shift. To operate in the 10¹⁶-cm⁻³ range, multiple-pass systems have been employed.

Electron temperature, or more generally the electron velocity distribution, can also be measured by electromagnetic-wave probing. According to hotplasma theory, effects arise at the second and higher harmonics of the electron cyclotron frequency given by $\omega_{ee} = eB/m_e$. These effects are attributable to the finite size of the electron gyration radius. The quasi-transverse extraordinary mode has been employed at 70 GHz to verify the predicted resonance width and depth. Conversely one could say that the resonance width and depth yield the effective temperatures parallel and perpendicular to the magnetic field in agreement with conductivity values.

Waves in plasmas are subject to a host of resonances at which the refractive index goes to infinity, such as at the ion and electron cyclotron frequencies and at hybrid frequencies. Much interest has been generated by the recent observations of such resonance



MICROWAVE INTERFEROMETER of "fringe-shift" variety.

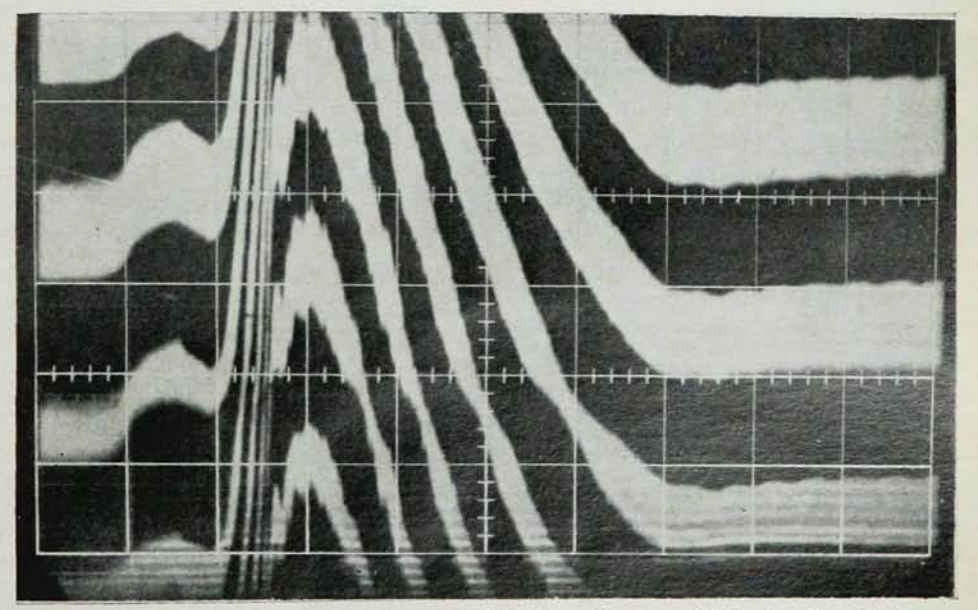
-FIG. 2

effects in the ionosphere, resulting in much theoretical work. Since such resonances involve **B** and n_e , a very useful diagnostic method is apparent, provided the experimentally observed resonances are correctly related to ω_{ee} and ω_{pe} .

Related phenomena occurring in the use of laboratory plasma probes have been known to exist for many years. For example, the application of rf signals to a biased probe will, because of the nonlinear nature of the probe characteristic, result in a greatly enhanced dc current component when ω

is near ω_p . The relationship between the resonance frequency ω_R and ω_p now appears clear, and experiments demonstrate agreement for n_v to within 10% of other measurements. The most versatile technique employed is that of ringing measurements wherein the probe is pulsed with a rapid-rise step function and the subsequent ringing of the probe-plasma system is observed. This allows determination of ω_R within a few periods and could be used to follow time-varying plasmas.

Transmission and reflection of short electromagnetic pulses (-10-9 sec) has



FRINGE-SHIFT density display from Model C stellarator. Peak density of five fringes is about 2.5×10^{13} cm⁻³. Time scale is 1 msec/div. FIG. 3

been used to determine the electron density. From analysis of the time shapes of the transmitted and reflected signals, both depending on ω_p , and observation of the transient ringing which approaches ω_p within a few cycles, n_e can be determined within a time smaller than 10^{-7} sec. In fact, this method was used to follow the decay of n_e in the afterglow.

Most of the measurements discussed above require only standard uhf and microwave components of relatively low power. The microwave bridge requires, for instance, a klystron of about 100 mW. Where absorption is severe and where background noise is high, backward-wave oscillators operating at frequencies up to about 100 GHz and many watts output are available. These tubes can be swept by about a factor 2 in frequency where resonance effects are to be sought.

PARTICLE BEAMS

Plasma measurement with particle beams has received relatively little attention, in view of the possible information plasma-beam interactions afford. If we exclude processes such as beaminduced instabilities and measurement of plasma electric and magnetic fields, the beam interacts not with the plasma as a whole but rather with individual constituents through binary collisions. Charged-particle beams can be used in plasmas when no magnetic field is present or if the plasmas are in open-ended magnetic devices. Atomic beams are better suited for probing when confining magnetic fields are present since plasma boundaries are better defined perpendicular to the field direction, and also since scattering by micro fields can be eliminated. We consider then two general classes of interactions and point out the merits of each.

Ion-atom interactions

An interaction that results in a gross change of state of the beam particle is the most easily detected. Such an interaction is charge exchange wherein an electron from a beam atom is transferred to a plasma ion. Charge exchange is not, of course, restricted to

ion-atom interactions but occurs also in atom-atom and ion-ion collisions. It is possible, however, to make charge exchange highly selective in practice. By this we mean that suitable choice of interaction energy and atomic beam can minimize the interaction with background neutral gas and plasma impurities relative to the ionic species of interest. Restricting ourselves specifically to what is termed resonant charge exchange (electron transfer between identical energy states such that the energy difference $\Delta E = 0$) selectivity becomes possible because of the energy dependence of the reaction cross section: $\sigma_r = a - b \log E$ where a and b are constants. The charge-exchange cross section for unlike atom-ion combinations, where $\Delta E \neq 0$, reaches a maximum at relative interaction velocities near the orbital electron velocity $(v \ge 10^{8} \text{ cm/sec})$ but decreases rather rapidly at low energies. For example, if we consider the case of a hydrogen atomic beam of a few thousand electron volts passing through a hydrogen plasma, the cross sections for electron loss or capture by the atomic beam interacting with background hydrogen gas is a factor 20 smaller than the resonant cross section between hydrogen atoms and protons.

If we choose a beam velocity large compared to the plasma ion velocity, say a few thousand electron volts for an atomic hydrogen beam (for which the detection is greatly simplified relative to the thermal energy range), and can restrict the k possible interactions to just atom-ion events, where charge exchange represents one such interaction, the relative interaction velocity v_r is constant and equal to the beam velocity v_B . The cross sections σ_k are constant and the attenuation of the particle beam due to the plasma can be expressed as

$$I = I_0 \exp \left[-\frac{1}{v_{\rm B}} \sum_{k} \sigma_k \, n_+ \, x \right] \quad (5)$$

where n_+ is the total ion density.

One envisions then a beam-transmission experiment for the measurement of ion density. Such experiments have been performed with hydrogen and helium plasmas for ion-density measurements. Comparison electron-density measurements have been made in both

cases. Spatial and temporal response is good (~ 1 MHz). For a plasma thickness of 10 cm the magnitude of the interaction cross section indicates the most convenient working density range to be 10^{13} – 10^{15} cm⁻³. In hydrogen plasmas consideration of the extent to which other ion-atom and atomelectron interactions lead to beam attenuation could be included and would constitute a small correction.

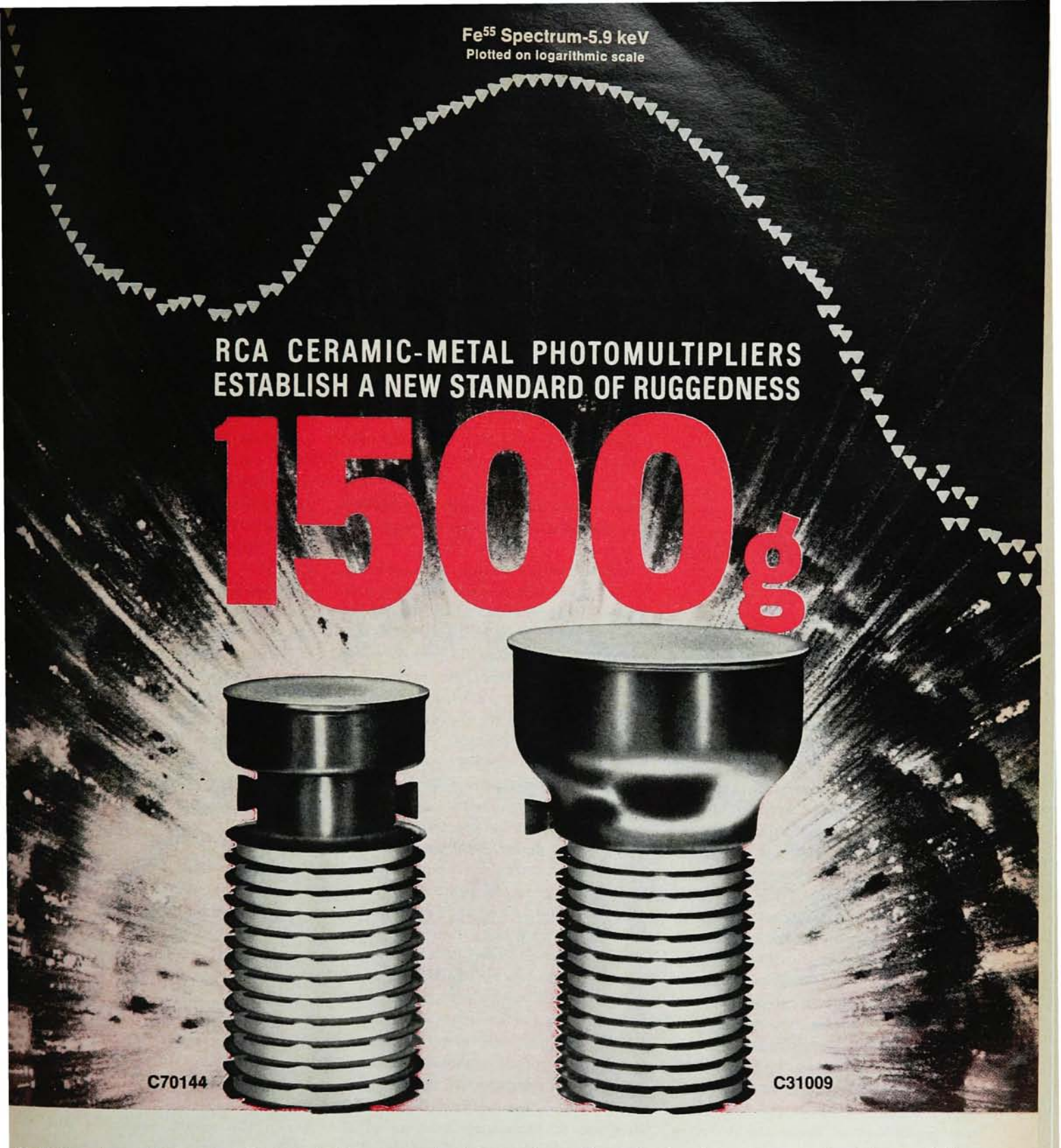
A thermal molecular hydrogen beam has been used for plasma density measurements although prior knowledge of the electron and ion velocity distributions was required since the relative interaction velocity arose solely from the plasma constituents. For deuterium plasmas an energetic tritium beam was employed for neutron production through the ³H (³H, n) ⁴He reaction. Maximizing this cross section requires about 0.1-MeV particle energies, however.

Another reaction is that of ion-atom elastic scattering. The long-range ion-atom interaction is given by the polarization potential

$$V = -\alpha e^2/2 \varepsilon_0 r^4 \tag{6}$$

where α is the electric-dipole polarizability of the atom. Subject to certain requirements on interaction energy, scattering potential and angular resolution of the scattering apparatus, the total atom-ion scattering cross section will exhibit a $v^{-2/3}$ velocity dependence over a wide energy range. With proper choice of beam and plasma these requirements can be met. Clearly resonant charge exchange, with its large characteristic cross section, is to be avoided. Possible combinations would be alkali beams and other alkali plasmas, helium beams and hydrogen plasmas, and hydrogen beams and helium plasmas.

An experiment not unlike that of Thomson scattering of a laser beam would allow determination of ion temperature by measuring beam scattering as a function of beam velocity. For a given distribution function $f(v_i)$, scattering will depend on v_B because $v_i = v_j - v_B$, allowing an ion temperature to be assigned. Best sensitivity occurs when beam and average ion velocities are approximately equal. Such an experiment is not easy since it requires



Now! New photomultipliers from RCA establish a new standard of ruggedness—shock: 1500 g at 0.2 ms; vibration: 60 g from 0 to 3,000 Hz—more than enough to withstand the rigors of rocket blastoff.

C70144, a 2" tube, and C31009, its 3" counterpart, are the first photomultipliers to be built without glass. Their construction consists of ceramic and metal wafers stacked alternately and bonded by brazing—with all materials selected for low radioactive content. Their aluminum-oxide window, with an almost perfect index of refraction of 1.78 for matching with NaI (Te) scintillators at 4100 angstroms, puts both photomultipliers into the priority class for detection and measurement of radiation on the moon, Mars, or more distant planets.

Variants of C70144 and C31009 for special requirements are also available. For example, the tubes can be made available with sap-

phire radiators for Cerenkov counting, and with low residual magnetic construction.

The new units are 10-stage, head-on types equipped with the RCA bialkali photocathode, providing low background and high quantum efficiency—28% typical, and in some cases as high as 40%.

C70144 and C31009 feature: minimum radioactive content, low dark current, and detection capabilities in the ultra-violet region of the spectrum. In addition to outer-space applications, both are suited for radiological surveys to log the "inner-space" composition of the Earth's strata.

For more information on these and other RCA Photomultipliers, see your RCA Representative. For technical data on specific types, write: RCA Commercial Engineering, Section G159Q, Harrison, N.J.

RCA ELECTRONIC COMPONENTS AND DEVICES, HARRISON, N.J.



The Most Trusted Name in Electronics

great alignment precision and presents difficult detection problems for nonalkali beams at low energies.

Electron-atom interactions

In electron collisions the relative collision velocity will nearly always depend on the electron distribution function. Ionization is the most easily detected interaction and cross sections for such events as functions of electron energy are now available for a host of atoms and some ions. Because of the cross-section velocity dependence, ionization rate coefficients $S_v = \sigma_v (v_r) v_r$, computed for Maxwellian velocity distributions, have strong electrontemperature dependence for $T_e \leq eV_1$, the ionization threshold. At higher electron temperatures there is relatively little temperature dependence. For beam probing of electron temperature one therefore requires separate knowledge of the electron density and a beam with an ionization threshold greater than the temperatures to be measured. Actually So peaks at about three times the ionization threshold so that a helium atomic beam might be used for electron-temperature measurements up to $T_e \approx 75$ eV. Of course, for a given electron density and beam path length in the plasma, the ionization cross section is best matched to the plasma in question when appreciable beam attenuation results. Occasionally, exceptions arise to these remarks concerning the temperature dependence of S_e. Notable are ionization cross sections of heavier alkali metals, which exhibit structure at electron energies well above the threshold due to autoionization levels. As a result the ionization rate coefficient of these atoms has a fairly strong temperature dependence out to about ten times threshold, that is, 30 - 40 eV. Beams of such atoms are then particularly well suited for the temperature range 2 - 30 eV.

Electron-temperature measurements have been made on stellarator discharges with potassium beams of about 3 keV. For typical stellarator discharges where $n_{\rm e} \approx 10^{13}$ the large ionization cross sections for the heavier alkalis afford good sensitivity whereas attenua-

tion of helium beams of such energies would be extremely small. In figure 4 we show a schematic of the beam apparatus and in figure 5 the response to a discharge in helium produced by a 5 kHz exciting voltage. Since the potassium beam is detected by secondary electron emission, the beam current is modulated at 100 kHz with band-pass detection to discriminate against emission from plasma ultraviolet light. From microwave measurements of electron density and potassium beam attenuation one can therefore solve for the electron temperature. The temperature modulation indicated here goes from 2.5 to about 7 eV, occurring at twice the discharge driving frequency but showing some asymmetry with the direction of the heating electric field.

Instead of ionization or scattering by electrons one can use excitation of a neutral atomic beam by measuring the excitation light. The difficulty encountered in practice here is low intensity since photons are emitted at all angles and only a very small solid angle can be used for detection.

Production of beams with large enough currents imposes no difficulty. Many ion sources available commercially have suitable current and voltage capabilities. The duo-plasmatron source of M. von Ardenne is the most efficient with respect to gas consumption. Neutralization of the ion beam by electron capture is quite efficient at moderate to low energies. When resonant charge exchange can be used, almost the entire ion beam can be neutralized down to thermal energies. Surface ionization sources can yield ion currents of about 1 mA per square centimeter of cathode area with cathode temperatures near 1500°K. Such sources are made by impregnating a base material (tungsten, rhenium or platinum) with an alkali metal of smaller work function. The "black magic" beta-eucryptites, such as Li2 CO3-SiO2-Al2 O3 can produce ions such as Li+ and Na+ as well as alkaliearth ions with the ease of electrons.

Detection of atomic beams is best accomplished by secondary electron emission when the beam energy is of the order of thousands of electron volts. At such energies the secondary electron coefficient will generally lie in the range 0.1 to 1.0 and either a bare

electron multiplier or a scintillatorphotomultiplier combination can be used. Both are quite sensitive to vacuum ultraviolet light and therefore some means of discriminating against plasma radiation is usually necessary. In some cases the atomic beam can be ionized with fair efficiency, thus rendering ultraviolet discrimination much easier since the beam can be deflected from the line of sight.

PROBES

The "simple single-wire" Langmuir probe is undoubtedly the most widely used diagnostic tool in plasmas even today. Such probes, though indeed rather simple mechanically, are quite the opposite in regard to the theory of current collection. In fact in most probe applications with plasmas immersed in magnetic fields, rigorous theory does not exist. Nevertheless probes continue to receive wide use since they can yield measurements with a degree of localization difficult to achieve by other methods. Even when operating in domains where approximations cannot be made to reduce the theory to a tractable form, they provide relative measurements that show a great deal of the structure of the usual nonquiescent plasma.

Collisionless plasmas

Probe theory for a collisionless plasma with no magnetic field is based largely on the original work of I. Langmuir and H. Mott-Smith. The treatment uses the concept of the Debye shielding distance $h = \left[\epsilon_0 \ k T_c / n_0 \ e^2 \right]^{1/2}$, which represents the distance over which a potential perturbation within a plasma decreases by a factor e, Te being the electron temperature and no the electron (plasma) density. This theory covers two domains. The first is that in which the sheath associated with the probe's electric field has thickness of order h, which is small compared with the probe radius; particles attracted through the sheath boundary by application of a probe potential V are captured by the probe in accordance with $I = j_r A_s$ where A_s is the sheath area as given by the Langmuir-Blodgett relationships for space-charge-limited current flow. jr is the random current density at the sheath boundary which, for a Maxwellian velocity distribution is

$$j_r = n \frac{\langle v \rangle}{4} = \frac{n_0}{2} \left(\frac{2 k T}{\pi m} \right)^{\frac{1}{2}}$$
 (7)

where T and m refer to the particle in question and j_r is the particle-current density.

If electrons and ions within plasmas were sufficiently coupled energetically to ensure that $T_e \approx T_1$ then equation 7 would apply to either type of particle. Ion-electron equipartition times are, however, often long compared with respective lifetimes, and because different cooling mechanisms operate on the two species, T1 and Te are usually quite different, the more common behavior being that $T_1 \ll T_c$. For this condition equation 7, when applied to the ions, does not yield sufficient ion current at the sheath edge for stability. The ions must approach the sheath boundary (insofar as a definite boundary exists) with a drift velocity given by $v \ge (2kT_e/m_+)^{1/2}$.

The saturated ion current for large negative potential V is therefore insensitive to the ion temperature T_+ , being

$$I_{+} \approx \frac{n_0 A_a}{2} \left(\frac{k T_o}{m_+} \right)^{\frac{1}{2}} \tag{8}$$

where A_a is the probe area. The possibility of direct information on ion temperature is thereby removed. That equation 8 is independent of probe voltage V implies that the result is approximate. The use of a probe to draw ion saturation current, although more complicated in theory than its electron counterpart, has the experimental advantage that the current is much smaller thereby imposing less perturbation on the surrounding plasma. Furthermore in even weak magnetic fields the electron current is so drastically altered that the ion current must be used.

The second part of the Langmuir theory treats the situation in which the sheath thickness is large compared with probe radius. Since most probes are made small (0.1 cm is a typical dimension) to minimize the perturbation, and the Debye distance is about 0.02 mm for $T_{\rm e} = 10 \text{ eV}$, and since $n_{\rm o} = 10^{12} \text{ cm}^{-2}$, this domain pertains to rather dilute plasmas.

While the respective particle fluxes yield the product of density and temperature (usually T_c), the dependence of probe current on voltage in the

transition region, where currents of both charge species are drawn, offers information on the electron temperature directly. In this voltage region part of the electron current is reflected, and the number of electrons going toward the probe are determined by remote collisions; therefore the electron distribution should be in thermal equilibrium. The density is then

$$n = n_0 \exp\left(-eV/kT_c\right) \tag{9}$$

where V is, of course, the probe potential relative to the plasma. The electron part of the probe current is given by equation 7 where n is evaluated at the probe surface of area A_a . From equations 7 and 9,

$$I_{\rm e} = A_{\rm a} \, n_0 \left(\frac{k \, T_{\rm e}}{2 \, \pi m} \right)^{\frac{1}{2}} \exp \left(-eV/k \, T_{\rm e} \right)$$
 (10)

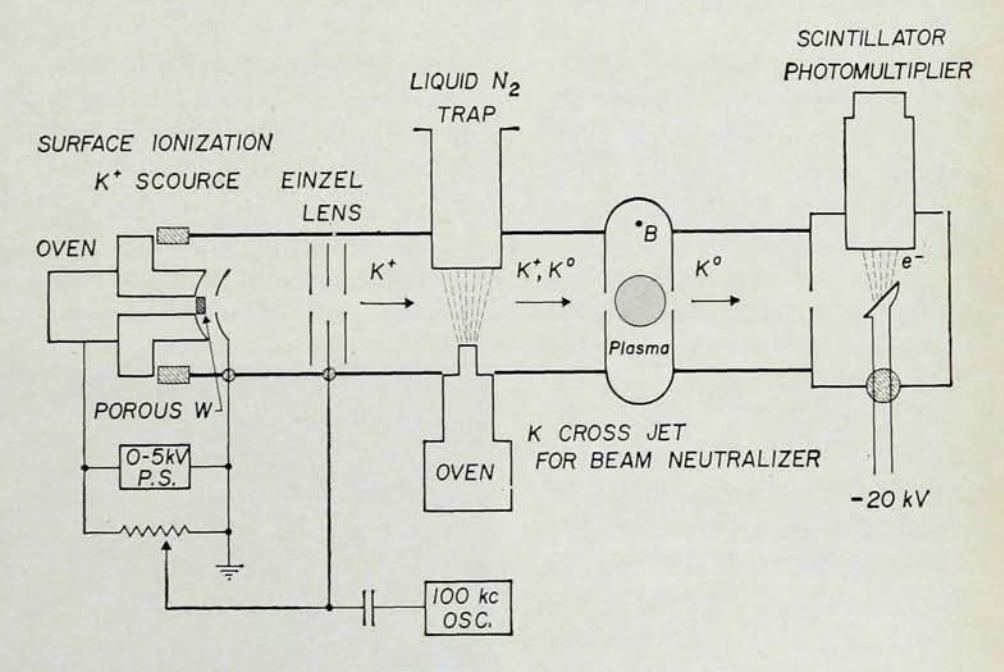
and a plot of $\log I_e$ as a function of V then gives a straight line with a slope that yields the electron temperature.

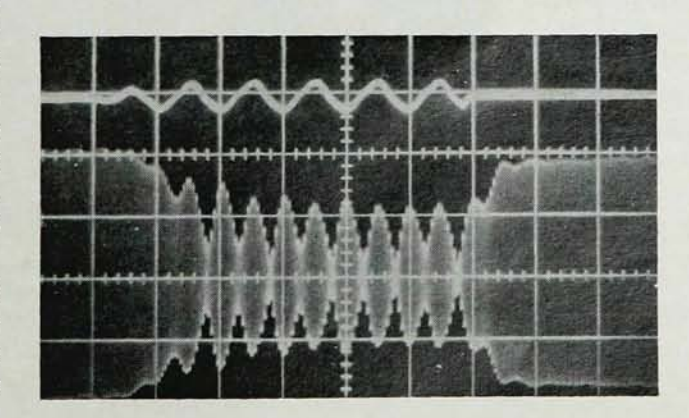
Since the total measured current I will contain I_+ , the plot should be $\log (I - I_+)$ against V.

Plasma with magnetic field

Application of a magnetic field B has the immediate effect of decreasing the ratio of electron to ion saturation currents. This ratio, which for B = 0 is $(T_e \ m_*/T_1 \ m_e)^{\frac{1}{2}} \approx 100$, can decrease by an order of magnitude when the magnetic field is such that the probe radius a and Debye length h are large compared to the electron Larmor radius re but still small compared to the ion Larmor radius r_+ . Whereas the electron current that is normally available with B = 0 is that diffusing into a surface surrounding the probe of radius equal to one mean free path, electrons in a magnetic field can move into the

POTASSIUM BEAM system for electron temperatures. —FIG. 4



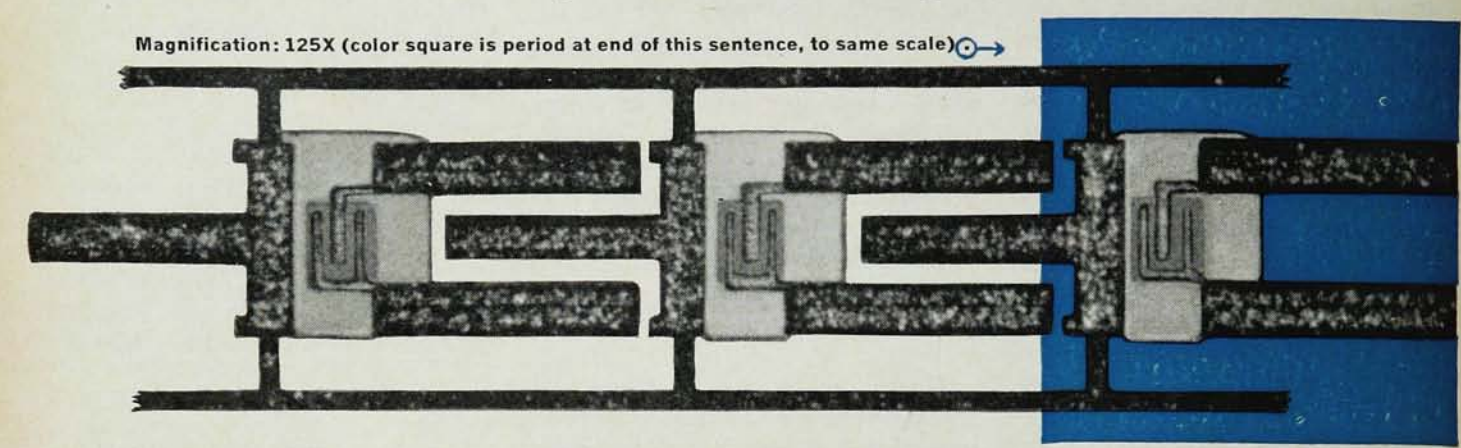


RESPONSE to helium discharge from B-1 stellarator driven at 5 kHz, showing potassium-beam attenuation. Discharge current is at top, beam intensity at bottom. Time scale is 200 microsec/div. Beam current modulation is 100 kHz. —FIG. 5

Report from

LABORATORIES

"Beam lead" technique for fabricating solid-state devices



Row or "ladder" of beam-lead transistors fabricated experimentally at Bell Laboratories has a transistor every 16 mils along its length. Each transistor (on light-gray areas) has three beam leads (dark-gray rectangular areas) for electrical and mechanical connection. The side rails at top and bottom of photo are used only for support and ease of handling.

To make tiny solid-state devices and circuits, groups of elements are generally formed on a single semiconductor slice or substrate. Then the slice is "diced" (physically separated) into pieces as either individual units or groups of units for integrated circuits. If used individually, they are connected to terminals or to other devices with short segments of extremely fine wire—a difficult and time-consuming operation. If used as groups of devices, they often need special processing to electrically isolate those making up each circuit.

Bell Laboratories' M. P. Lepselter has developed a promising solution to both of these problems. After the device elements are formed, mechanically strong electrical leads are deposited onto them. These electrically and mechanically intraconnect the devices and circuits. Unwanted semiconductor material between the individual devices in a circuit is then removed . . . isolating them electrically, yet leaving them mechanically

joined. This permits batch processing of electrical leads, eliminating many individual connections and requiring only connection to external terminals.

Thus, handling tiny devices and circuits is simplified. The leads, precisely positioned with respect to each other, are easily connected to a circuit board or other support, perhaps eventually by automated techniques. They are strong enough so that the semiconductor wafer or chip needs no further attachment to the substrate. Entire circuits joined by beam intraconnections can be handled as one unit.



M. P. Lepselter examines beam-lead model (enlarged about 300 times). Beams were thermally aged in 360° C steam for 1000 hours, centrifuged to 130,000 G, bent 90° twenty times without failure. Beams can be tapered for smooth impedance matching, widened to act as heat sinks.



probe only along the direction of the field. Electron motion along the field is essentially unhindered whereas across the field the diffusion coefficient is reduced (classically) by the ratio $D_{\perp}/D =$ $1(1 + \omega_{ce}^2 \tau^2)$ where $\omega_{ce} \tau = (eB/m)$ $(1/n_0\sigma v)$ is the product of the electron cyclotron frequency and mean collision time with ions or neutrals, whichever is dominant. For even very low fields weet >> 1; hence classical diffusion varies as $1/B^2$ and becomes extremely small. Classical diffusion is seldom observed in practice, the cross field diffusion being given rather by the Bohm expression which varies as Te/B. Nevertheless, electron collection is mainly along the flux tube of radius $a + r_e$, with diffusion across the entire tube boundary maintaining the particle flux.

Electron collection is treated by D. Bohm⁹ who obtains an expression with a correction factor varying as the square root of the transverse diffusion coefficient.

Subject to the initial approximations, namely that the ion cyclotron radius is still large compared to a and h, the saturated ion current is still given by equation 8.

Interestingly enough, recent extensive experimental work comparing probe-deduced values of n_e and T_e with microwave and conductivity values shows rather good agreement with probe theory. The theory referred to, however, is for B = 0 although the measurements were made at about 35 kG where both electron and ion cyclotron radii are less than the probe size. Specifically, the ion current is taken to be the Bohm value $I_{+} = 0.4 n_0 A$ $(kT_o/m_+)^{1/2}$ but with A equal to twice the probe area perpendicular to the magnetic field. Similarly the electron current is the random value given by equation 7.

Well defined probe characteristics are obtained whereby both ion and electron currents saturate ($n_e \approx 10^{13}$ cm⁻³ and $T_e \approx 10$ eV). It was found that drawing electron saturation currents increased the plasma floating potential along the lines of **B** as detected by a second probe downstream. The resulting corrections to the space potential and T_e were about 10%.

The probe value of T_e appears consistently high relative to conductivity values, the discrepancy being at worst a factor of 2. Since the conductivity measurements have been well established by other means, notably spectroscopic, it must be assumed that probe temperatures are in error. Furthermore if the lower conductivity temperatures are used in determining the plasma density, better agreement (to within $\sim 20\%$) is obtained between probe and microwave.

In any case the probe remains invaluable for relative and highly localized measurements. From a 24-probe azimuthal array K. Bol¹⁰ has produced a beautiful display (figure 6) of density fluctuations occurring for given operating conditions of the Etude stellarator.

Double probes

Single-probe characteristics rely on establishment of a firm plasma potential that serves as a reference for the probe voltage. In some discharges a good reference point does not exist and in others fairly large electron currents, drawn to establish the probe characteristics from which the space potential can be deduced, cause perturbations sufficient to alter the plasma conditions. The double-probe system was proposed to alleviate this difficulty. Two probes are spaced sufficiently close to ensure uniform plasma in the intervening region. The probe system is allowed to float relative to the plasma so that no net current is drawn by the system. The resulting potential is the "floating potential," which is sufficiently negative with respect to the plasma to repel enough of the higher mobility electrons to maintain $I_e = I_+$.

Between the probes one places a bias $V = V_1 - V_2 > 0$. Positive current flows in the external circuit from probe 2 to probe 1. If the probe areas are such that $A_1 \approx A_2$, both probes are negative relative to the plasma but V_1 is less negative and V2 more negative. Thus more electrons flow to 1 and fewer to 2. For large positive V, probe 2 will draw only ion saturation current while probe I collects just enough net electron current to cancel the ion current to 2. The double-probe characteristic is thus symmetric when $A_1 = A_2$ and the total current to either probe cannot be greater than the ion saturation current. This condition has the advantage of minimizing the plasma perturbation since the current flow is small; at the same time, however, only the electrons in the tail of the distribution enter the probe current.

Gridded probes

Devices of the sort to be described briefly here should probably be referred to as particle analyzers" rather than probes since they attain a size such that the term "localized, nonperturbing measurement" can hardly be ascribed. We refer to multigrid, retarding-potential probes, which because of the mechanical requirements must attain a size of the order of centimeters. Such probes have been used in satellite measurements and in laboratory plasmas for particle-velocity distributions. Generally too large to thrust directly into a plasma, they are best adapted to regions that are loosely coupled to the main plasma body where there is a minimal perturbing

The interpretation of the probe is simplified when the entrance slit or grid spacing is small compared to the Debye distance ensuring penetration of imposed electric fields throughout the sampled plasma. Particle flow along the magnetic field has the advantage that the potentials cannot seriously defocus the entering beam. Retarding-potential analysis of either particle species can be accomplished with the opposite species biased off, thus giving the energy distribution of either type of particle.

Measurements made in the divertor of the Model C stellarator with a fourgrid probe yield ion and electron temperatures in good agreement with other diagnostics. The grids are encased in a metallic housing having an entranceslit width of 12 microns (- 1/4 the local Debye distance for a typical plasma density in the probe region). The device operates in a field region where the magnetic field expands to the value $B_{\rm D}$, where $B_{\rm D}$ is about 1/4 of B_0 , the main stellarator field. As a result the local velocity distribution of escaping particles is distorted (collisionless treatment) such that the velocity perpendicular to B is reduced and that parallel to B is increased. The transparency of the grids and entrance slit is thereby

improved. The resultant expression for the current (either species) is

$$I = C \left[\frac{B_0}{B_D} \exp\left(-\frac{ZeV}{kT}\right) - \frac{(B_0 - B_D)}{B_D} \exp\left(-\frac{ZeV}{kT} \cdot \frac{B_0}{B_0 - B_D}\right) \right]$$
(11)

where the constant C contains geometrical factors and V is the retarding voltage for the species in question. The second term of the equation arises from the expansion of the magnetic field. Shown in figure 7 is the collector current I plotted against ZeV/kT. The departure from linearity of log I at small ZeV/kT arises from the effect of the expanding magnetic field. The points are measured values for electrons in an ohmically heated stellarator discharge where $n_e \approx 10^{13} \text{ cm}^{-3}$ and $T_e \approx 20$ eV. The slope of such distributions allows evaluations of Te that are within 30% of the conductivity values. Furthermore the energetic part of the distribution can be examined in detail for evidence of non-Maxwellian particles.

Ion distributions show, in addition to the exponential region, a flat domain for $0 < V \le 3 \ kT/eZ$ which is attributed to a sheath of ions accelerating toward the wall. The only discrepancy between the actual performance of the probe and that calculated was in the transparency of the grids. The geometrical value, corrected for the computed particle orbits, was a factor 1/2 higher than the measured value, a small correction in itself that introduces a factor 2 error in absolute flux determinations when raised to the fourth power for the 4-grid assembly.

Magnetic probes

Magnetic probes have been treated by Lovberg¹² who points out their widespread use in mapping current distributions in plasma accelerators and pinches. We would add to this some discussion of a special case in which the currents are "diamagnetic" and the probe is therefore termed "the diamagnetic probe." We recognize that the discussion that follows is applicable

only to transient plasmas or steadystate plasmas that can be modulated.

The plasma has a magnetic moment per unit volume

$$\mathbf{m} = -\frac{p_{\perp}}{R^2} \mathbf{B} \tag{12}$$

where p_{\perp} is the pressure perpendicular to the magnetic field and is given in terms of plasma density n and ion and electron temperature by $p_{\perp} = nk(T_{+} + T_{e})$. If we take **B** along the z axis and consider a plasma section of radius r_{p} and thickness dz, the magnetic moment per unit volume is

$$dM_z = -\pi r_p^2 \left\langle \frac{p_\perp}{B_z} \right\rangle dz \quad (13)$$

and can be expressed in terms of a solenoidal current $I=I_{\rm D}\ dz$ where $I_{\rm D}$ is the diamagnetic sheet current density. Then

$$dM_z = \pi r_p^2 I_D dz \tag{14}$$

where $I_{\rm D} = -\langle p_{\perp}/B_z \rangle \approx -\langle p_{\perp} \rangle/B_0$ and where we substitute the vacuum field B_0 for B_z on the assumption that the ratio of plasma pressure to magnetic pressure $\beta \ll 1$.

A single-turn loop of radius r_L surrounding the plasma column will have an induced voltage in accordance with

$$V = -\frac{\partial}{\partial t} \int B_z dS \tag{15}$$

and if fluctuations in B_z can be neglected (usually subtraction by a second coil which does not encircle the plasma affords the best means of cancelling this term) then

$$V = \mu_0 \pi r_p^2 \frac{dI_D}{dt}$$
 (16)

We assume uniformity of p_{\perp} with r and z. In general, p_{\perp} may vary in both dimensions.

When the plasma is concentric within a metal-wall vacuum system the time rate of change of the diamagnetic sheet current $dI_{\rm D}/dt$ will induce an emf in the wall and cause a wall current $I_{\rm W}$ to flow. $dI_{\rm W}/dt$ thus contributes to V in a manner that depends on the wall time constant. Wall effects must therefore be included,

Diamagnetic probes have been put to greatest use in ion- and electroncyclotron-heated plasmas where the perpendicular pressure or temperature is often much greater than its counterpart along the magnetic field. The energy distributions are frequently not Maxwellian and the pressure measurement serves only to give the mean energy density $n(\varepsilon)$, or nkT_{\perp} if one wishes to assign a temperature to the distribution.

It has become common to use rapid scanning techniques for electric probes. The need for this arises from the highly transient nature of many plasmas and the destructive power that flows into probe tips with dc voltages. Even for steady-state plasmas the sawtooth voltage scan, which requires only a few microseconds to complete, allows continuous oscilloscope display of the probe characteristic as plasma profiles are studied. Furthermore, the widespread use of both electric and magnetic probes for fluctuation measurements as they relate to the identification of instabilities is facilitated by spectrum analyzers, variable band-pass filters, and communication receivers.

LASERS

Lasers for plasma diagnostic measurement are becoming increasingly popular. The most vigorously pursued experiments of recent years involving plasmas and lasers have been efforts toward observation of Thomson scattering of the laser photons by plasma electrons. Although such experiments were always possible in principle, the smallness of the Thomson cross section ($\sim 6 \times 10^{-25}$ cm²) required the introduction of lasers to yield sufficient scattered photons relative to background light and phototube noise to give meaningful results.

The scattered spectrum depends on a parameter a defined as the ratio of Debye distance to the wavelength of the sinusoidal plasma-density fluctuation. For $\alpha \gg 1$, coherent plasma oscillations can exist that give structure to the scattered electromagnetic wave; the central line of scattered radiation has a width characteristic of ion Doppler broadening, and has satellite lines separated from it by approximately the plasma frequency $\pm \omega_p$. Under these conditions the electron density can be inferred from ω_p . When $\alpha \ll 1$, only a central peak of scattered radiation is observed with a width characteristic of electron thermal motion. Absolute intensity measurements can yield the electron density.

For hydrogen plasmas α is given in terms of scattering angle θ as

$$\alpha = 1.58 \times 10^{-13} \,\lambda_0 \left(\frac{n_e}{T_e} \, \frac{1}{1 - \cos \theta} \right)^{3/2}$$
(17)

where λ_0 is the wavelength of the incident radiation in nanometers, n_e the electron density, and T_e the electron temperature ($T_e = T_+$) in eV.

Within the last two years many experimental observations have been reported employing plasmas of density 10^{16} to 10^{16} cm⁻². These experiments span the region $\alpha = 1$ by varying the scattering angle. Some evidence for satellite lines is observed for forward scattering where $\alpha > 1$. Agreement with other diagnostics, when available, is fairly good.

Although it appears that the rewards are potentially great, Thomson scattering is a difficult experiment at best, requiring great care in minimizing the background signal. Ruby lasers operating in the giant-pulse mode and delivering tens of megawatts of power are necessary to resolve the scattered signal. At present it is rather like the tail wagging the dog.

SPECTROSCOPY

A tremendous number of spectroscopic methods is available for determining plasma properties. Were most plasmas not quite so tenuous, the determination of electron and ion temperatures and number densities would be considerably simplified. If, for instance, the excited populations of atoms and ions within the plasma were determined solely by collisions and the system responded instantly to changes in plasma conditions, the plasma would be said to be in local thermal equilibrium (LTE). Each collision process has its inverse and these pairs of processes would occur at equal rates. Free electrons would have a Maxwellian velocity distribution, and the bound-level populations would be given by the Boltzmann and Saha equations.

For the plasma to be in LTE the collision deëxcitation rates should then be at least a factor 10 larger than radiative decay rates, a requirement which for hydrogen and helium plasmas is most stringent for the low-lying states where radiative lifetimes are short. As cross sections for excitation are gen-

erally larger than those for deëxcitation the population of a given lowlying level q in LTE is then determined primarily by collision-induced transitions from levels where $E_p > E_q$ balanced by collisional excitation from q to all levels where $E_p > E_q$. Only in dense low-temperature plasmas such as in pinches and shock tubes will lowlying excited states be in LTE.

Temperature is readily determined from the intensities of spectral lines arising from a common lower level and two upper levels. The weakness of this method, though, is that the level spacing becomes small between excited states. That is, $E_p - E_q \approx kT_e$ and the temperature sensitivity is low.

When relative line intensities of subsequent ionization stages of a given element can be compared, much stronger temperature sensitivity is achieved due to the appearance of the ionization energy in the exponent. These methods and the domain of validity of LTE are considered in detail by H. Griem.²

The ratio of line-radiation to continuum radiation which arises from radiative recombination and bremsstrahlung has a rather wide temperature range of good sensitivity. Beyond a lower temperature limit, however, the negative-ion continuum must be included. For neutral helium, line-tocontinuum ratios can be used in the temperature range below that for which recombination and bremsstrahlung in doubly ionized helium are important. This defines a range of about 1 to 3 eV. When T_c is such that $n(\text{He}^{++}) \ge 10n \text{ (He}^{+}) \text{ this procedure}$ can again be used for He II spectra (from He⁺) where $8 \le T_e \le 50$ eV.

As the electron density is lowered, radiative decay and recombination become dominant over collision effects. When states depopulate primarily by radiative decay, balance is not maintained by the inverse process in optically thin plasmas and LTE ceases to apply. At this extreme of low density the steady-state corona model applies and the degree of ionization is governed by ionization and recombination coefficients; that is, it depends on specific knowledge of atomic parameters.

The ion distribution is independent of electron density, and population densities of excited states of these ions are balanced by collision excitation and spontaneous radiative decay. Establishing the equilibrium distribution requires a finite time, however, which is longer than the lifetimes of most transient plasmas. Consequently, such plasmas could not be characterized by an equilibrium corona model. One is therefore forced to differential equations for the ion and excited-state populations which include not only rate coefficients for excitation, ionization and recombination but the influx and loss of particles in the various ionization states as well. These equations get rather unwieldly for hand calculation but can be conveniently handled on a computer to obtain best parametric agreement with the experimental quantities relating to ne, Te, n(Z, p), etc.

For the transition region of electron density where radiative lifetimes of highly excited states are of the order of collision times, a collision-radiative (CR) model that includes stepwise collision processes and three-body recombination has been introduced. The differential equations defining the populations now contain summations over not only radiative effects but collision processes as well. The summations can, however, be finite since for very highly excited states the radiative effects can be neglected, the CR model going over into LTE.

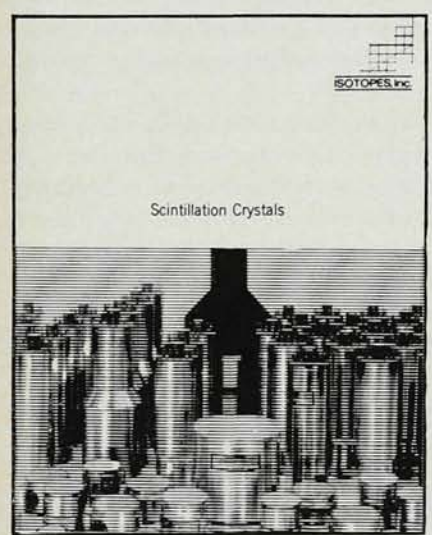
When absorption of radiation occurs within the plasma the population densities are modified, and the intensity observed is not the incremental sum along the line of sight. For transient, moderately low-density plasmas the ground-state population dominates over the excited-state populations and absorption of line radiation first becomes important for the resonance radiation.

A general solution of the equation of radiative transfer is not available because the source function depends, in many cases, on the spectral line shapes. When ion self-collision times are short compared to radiative lifetimes, an emitted photon bears no relation to a previously absorbed photon, and the source function is frequency independent.

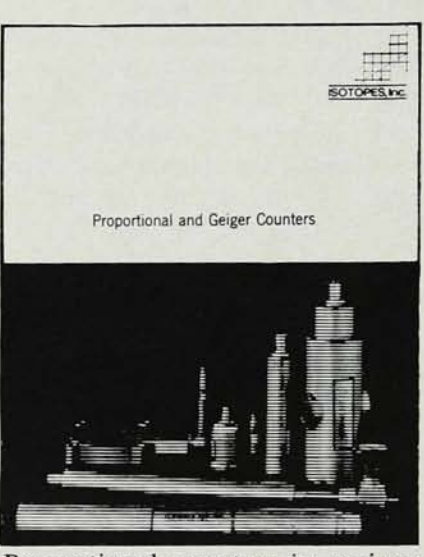
The free-free transitions of a uniform proton-electron plasma give for emission and absorption a relationship

Got a question on scintillation crystals, proportional and geiger counters, or solid state detectors?

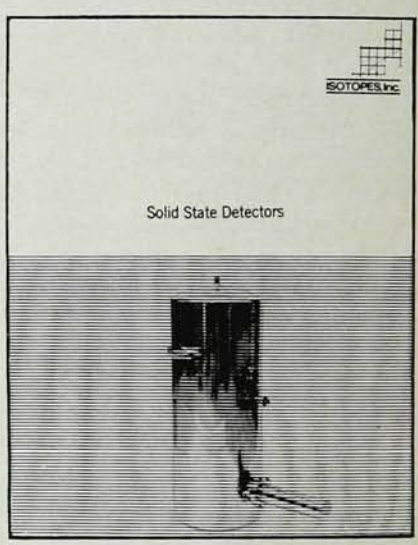
We've got the answer.



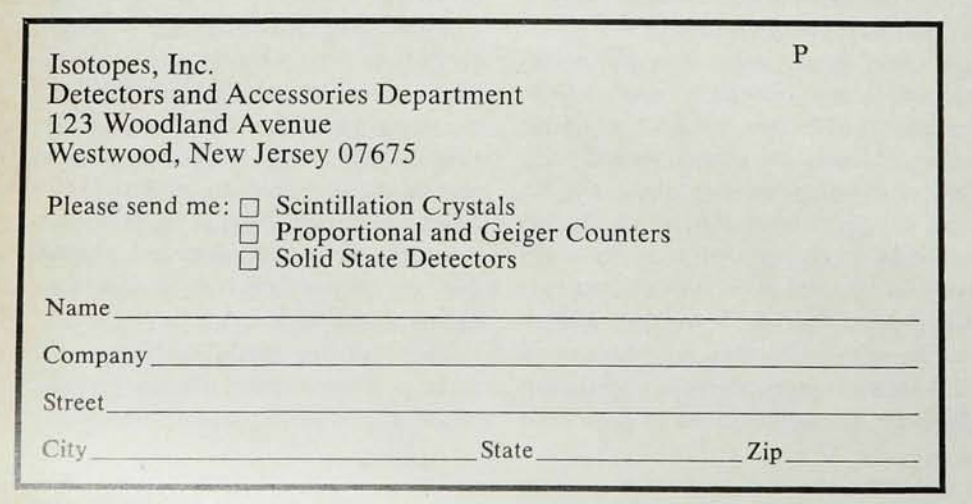
This, the newest of our detectors catalogs, gives specifications, performance data and prices for the standard, integral and unitized series crystals manufactured by Isotopes, Inc. Full specifications on special NaI(Tl) crystal units such as low background and thin crystal assemblies, hole-through crystals and mosaic assemblies, and high-altitude units are also given.

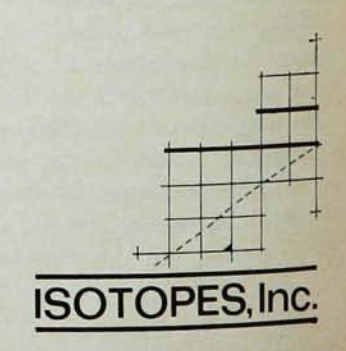


Proportional counters in various configurations, G-M tubes, low-background flow counters, flat anti-coincidence counters, gas-sampling tubes, neutron-beam monitors and BF₃ neutron detectors are described in this catalog. Various combinations of window and cathode materials for specific custom modifications are also included.



Our solid state detectors catalog details our line of lithium-drifted germanium and silicon detectors. Complete specifications as well as prices are listed for detectors with active volumes up to 20 cubic centimeters, areas ranging from 6 to 20 square centimeters and depletion depths up to 10 millimeters. Complete information on electronic components specifically designed for use with these detectors is also included in the catalog.



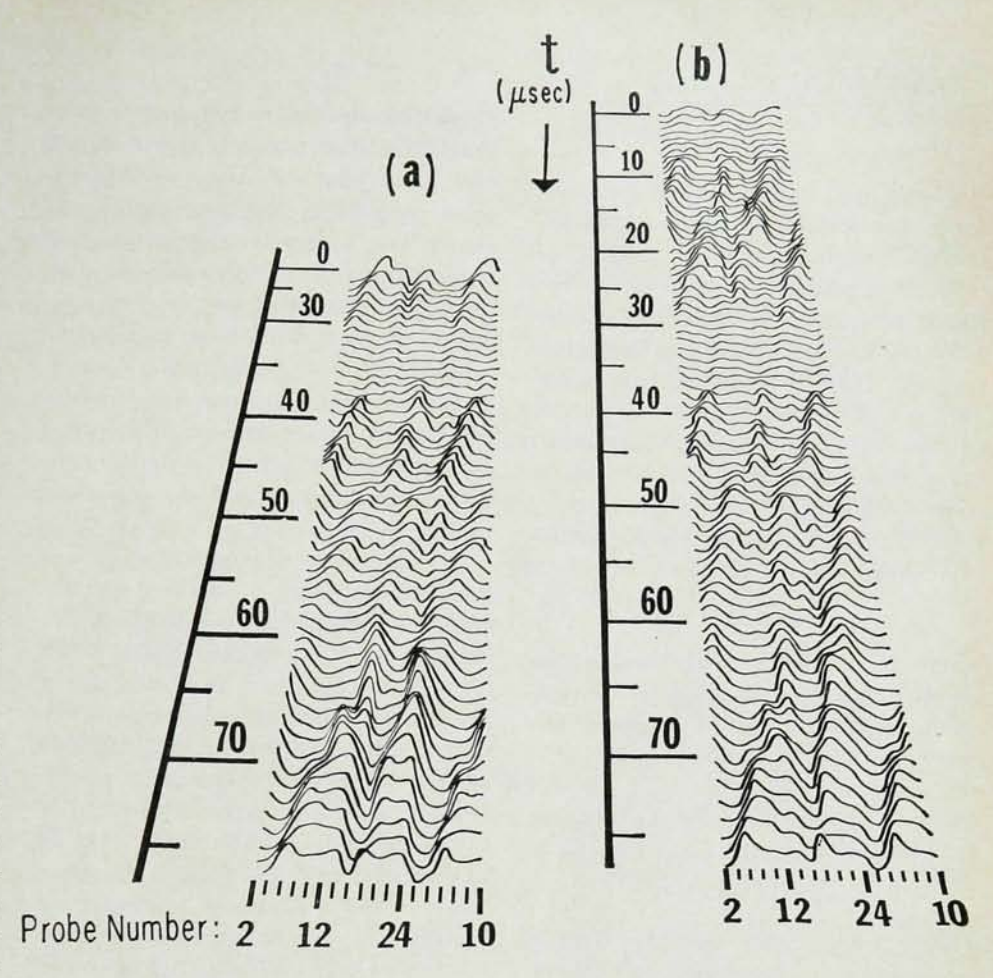


which, for $h_r/kT_c \ll 1$, shows that the absorption coefficient approaches 1/v2, becoming very large for small v, so that the spectrum approaches that of a black body having a temperature Te. From relative measurements of radiant intensity J_{ν} as a function of ν in the long-wavelength region, the electron temperature can be found. The restrictions imposed on such measurements are rather severe, however. The frequency interval is bounded on the low side by the plasma frequency ωp and on the high side by departures from black body intensities. For measurements to date, a range of about a factor 10 in wavelength has been available. Since the temperature measured corresponds to that of about one absorption length beneath the surface, the method relies on plasma homogeneity and requires rather large, high-density plasmas. Absolute intensity measurements in the optically thin region can yield the electron density. If the plasma frequency is observable by the radiation detector, the density follows automatically.



Recent development of photodetectors for the far infrared now allows, for this spectral region, detector-response times near those of visible-light detectors. These are based on photoionization of impurity atoms or excitation of free carriers in the semiconductors germanium and indium antimonide. Being photoconductive devices, these detectors require a threshold photon energy and operation in a low-temperature bath near liquid-helium temperatures. The Putley detector (InSb) requires a magnetic field to yield optimal performance but can be used to wavelengths greater than 1 mm.

In the visible region of the spectrum similar techniques can be employed for determining T_e . The line-intensity-ratio method mentioned earlier, and the intensity variation of the continuum arising from the factor exp $(-h_v/kT_e)$, can be used in principle. For sensitive temperature dependence h_v should be greater than or of the order of kT_e , so that the methods are



FLUCTUATIONS in azimuthal density from 24-probe assembly on Etude stellarator. (a) total signal, (b) frequencies above 25 kHz. -FIG. 6

best suited for $kT_{\rm e} \leq 10$ eV. From intensity considerations of the continuum, densities of at least 10^{14} cm⁻³ are necessary.

Under time-dependent-corona-model conditions the lifetime of a given ion can be used to estimate electron temperature provided the temperature is relatively constant over the observation time. Since absolute calibrations are not required, the method is attractive where feasible. R. W. P. McWhirter¹³ has calculated the time history for Balmer lines on Zeta for varying temperatures and initial densities of hydrogen atoms. The range of applicability is $2 \le T_e \le 30$ eV and $n_e < 10^{15}$ cm⁻³.

L. Heroux has used the line-ratio method for lithium-like ions for which the intensity ratio is independent of n_e and the ground-state population. The lithium-like ion chosen was N V (quadruply-ionized nitrogen) and the lines used were $\lambda = 209$ nm (2s -3p) and $\lambda = 123.9$ nm (2s -2p). Since the upper levels differ by 49 eV, good tem-

perature dependence is achieved to $T_{\rm e} \approx 100$ eV. The method has wide applicability when applied to the range of possible ions, C IV, N V, O VI, Ne VIII, etc.

Density measurement

So far we have concerned ourselves primarily with the problem of electron temperature. Many of these methods can yield electron or ion densities subject to absolute calibration of the recording instrument, a procedure not difficult for the visible and near ultraviolet regions of the spectrum. For hydrogen plasmas the continuum intensity can be predicted with good accuracy so that n_e and n_1 can be inferred from continuum intensities if one has even a very rough knowledge of T_e .

When plasma densities are sufficiently large, the most elegant means for determining n_e is Stark broadening. Theory is now sufficiently refined to achieve agreement with experiment for hydrogen, helium and some heavier

elements to an accuracy quite adequate for plasma-density determinations. Although the more accurate method of determining densities is to compare the measured profile with profiles calculated for a range of densities and select the best fit, it is a tedious procedure, and one frequently resorts to only a comparison of full width at half maximum. Calculated values can be taken from the tables given by Griem.² Specifically, the density is related to the full Stark widths $\Delta \lambda_s$ by

$$n_e = C(n_e, T) (\Delta \lambda_s)^{2/3}$$
 (18)

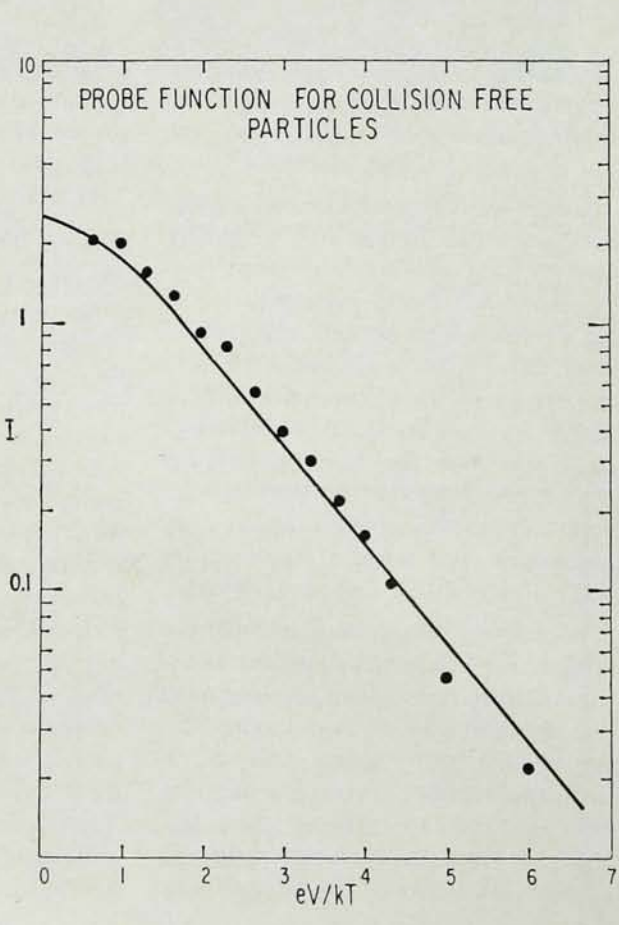
where C is only a weak function of electron density and temperature. For the hydrogen line H_{β} , C is essentially constant over the density range 10^{14} – 10^{15} cm⁻³ and $0.5 \le T_e \le 4$ eV. An estimate of the expected broadening using the value of C in equation 18, is

$$n_{\rm e} \approx 3.5 \times 10^{14} \, (\Delta \lambda_{\rm s})^{2/3}$$

which defines the working density range. Below $n_e = 10^{15}$ cm⁻² one will be increasingly troubled by Doppler effects, fine structure, Zeeman splitting.

From the above discussion it is clear that the instrumentation required need not be subject to stringent requirements regarding resolving power and dispersion; a wavelength accuracy of aproximately 0.1 nm usually is sufficient to define the radiating species and to perform Stark-broadening measurements for $n_e \geq 10^{15}$ cm⁻³. Consideration of sensitivity and time resolution are important because of the need for good statistics at the detector in times short compared to those of plasma variations.

It is always advantageous to have a good quartz prism or grating spectrograph for general survey work in the range 250 < λ < 800 nm. Quartz-prism instruments are more expensive for a given resolution. Whether photoelectric or film recording is best depends entirely on the usage. Generally photographic recording is useful primarily for wavelength measurements (that is, to determine species). It does not offer, however, the accuracy of photoelectric devices for intensity measurements. When intensity variations are to be observed or when conditions during a transient discharge are to be followed,



RESPONSE FUNCTION for gridded probe in expanded magnetic field, showing current *I* plotted against normalized retarding potential eV/kT. —FIG. 7

either photoelectric or moving films (drum camera or equivalent) must be used. For weak spectral lines the integrating property of film is an advantage. In transient repetitive discharges of good reproducibility, time resolution can be achieved with film recording by using synchronized choppers while retaining the integration properties.

Frequently the desired plasma properties can be adequately inferred from one or two spectral lines. For such single-line work the monochromator is widely employed in plasma measurements. Monochromators are nearly always grating instruments for economy in resolution and spectral range. Wavelength selection is made by manual or servo-driven grating rotation or detector motion in the focal curve. Detection is usually photoelectric.

When line profiles are required in transient discharges, as for Stark broadening, composite systems consisting of monochromator or spectrometer and streak camera are now available commercially. The latter component usually involves a rotating mirror and fixed film or rotating film drum to achieve the time resolution. Electronic image-converter cameras are available combining considerable amplification and sweep speeds of many centimeters per microsecond.

One exception to the above remark concerning the degree of dispersion generally required in plasma work arises when ion temperatures are desired from Doppler broadening. Since the spectral shift is given by $\Delta \lambda = \lambda$ $\lambda_0 = (v/c) \lambda_0$ where v is the velocity along the line of sight and c the velocity of light, a Maxwellian ionvelocity distribution yields a Gaussian line profile, where the full width at half maximum $\Delta \lambda_0$ is $(2kT \log 2/mc^2)^{\frac{1}{2}}$ λ_0 . Thus, at kT = 10 eV, $\Delta \lambda_D \approx 10^{-4} \lambda_0$ for hydrogen, so that one is interested in the line profile measurements over increments of 0.01 to 0.001 nm. Many techniques have been adopted to spread the emergent lines from monochromators so that multiple phototube detectors can be used to give the profile in time. Examples are cylindrical lenses, stacked arrays of very thin glass plates coupled to fiber optics, and rotatable quartz plates at the entrance or exit slits. For heavy low-temperature ions and weak spectra, the FabryPerot interferometer possesses marked advantages in resolution and lightgathering power.

Ultraviolet

In many plasmas, spectroscopy in the vacuum ultraviolet becomes necessary for several reasons. For nearly all ions the large energy differences between ground states and first excited states places resonance lines in this spectral region. Consequently, most of the radiant power and the more intense lines occur in the region below the quartz and oxygen cutoffs from 185 to 200 nm. Lithium fluoride retains transparency to about 110 nm, but has to be treated rather gently to maintain this lower limit, Calcium fluoride transmits from 130 to 140 nm only, but is more durable than lithium fluoride. Windows can often be avoided by vacuum coupling and differential pumping.

Of more serious nature is the loss in reflectivity of materials as the wavelength goes below 100 nm. For $\lambda < 50$ nm all known materials are such poor reflectors at near normal incidence that spectrometers must adopt the grazing-incidence geometry. As the angle of incidence approaches 90 deg, the reflection coefficient approaches unity. Grazing-incidence instruments generally employ incidence angles of 80 to 85 deg and can work down to 2 to 10 nm, depending on intensity.

Detection of radiation in the vacuum ultraviolet is frequently accomplished with a thin coating of sodium salicylate on the phototube face. The spectral response is relatively flat for $\lambda \geq 50$ nm but the detector system is sensitive to scattered light in the visible region. Thin plastic scintillators might also perform similarly. Bare-cathode electron multipliers have the advantage that they are not sensitive to photon energies less than the work function of the photocathode or dynode material. Several commercial tubes are now available with lithium-fluoride windows and cesium-telluride and cesiumiodide photocathodes which give narrow spectral responses of 110 to 350 nm and 110 to 180 nm, respectively. These were developed primarily for rocket research.

X-rays

Spectral exploration of the x-ray region (0.1 to 5 nm) has been rather limited

in laboratory plasmas due to the requirement that kT be about 100 eV or more for sufficient working intensity. Although considerable experimental work in this region has been done on solar-corona radiation, notably by the US Naval Research Laboratory, laboratory plasma work has come primarily from the Los Alamos work with theta pinches.

Radiation in this region will contain contributions from three sources (assuming the presence of some relatively high-Z impurities):

Free-free (bremsstrahlung) radiation where the emission per unit frequency interval varies as

$$\sum_{i} \frac{n_{e} n_{i} Z^{2}}{(kT_{e})^{\frac{1}{2}}} \exp(-h\nu/kT_{e}) \quad (19)$$

where the sum extends over all ions present in the plasma.

Free-bound (recombination) radiation which for capture into hydrogenlike states by stripped ions has the form

$$\frac{dE/d\nu \approx [n_{\rm e}n_{\rm i}Z^4/(kT_{\rm e})^{3/2}]}{\times \exp[-(h\nu - X_{\rm q})/kT_{\rm e}]}$$
(20)

where X_q is the ionization energy from state q of the ion in question.

Bound-bound (line) radiation by incompletely stripped ions.

The important thing from the standpoint of plasma diagnostics is that both free-free and free-bound radiation have frequency dependencies, for $h\nu \gg kT_e$, governed by the exponential and are admirably suited for temperature measurement. The extent to which the continuum measurements are confused by line radiation depends on the plasma constituents. If oxygen is the heaviest serious impurity, its series limit (O VIII) is at 1.42 nm, below which only the continuum is observed.

Spectral analysis has been accomplished by two different means. The first is absorption measurement, which, while cruder in wavelength discrimination, can subtend moderately large solid angles if intensity is a problem. If the spectrum is essentially pure bremsstrahlung, then a relative measurement of the intensity through two absorbers suffices to determine $T_{\rm e}$.

More detailed spectral analysis is possible with crystal monochromators. These operate by reflection near the Bragg angle $(n\lambda = 2 \ d \ \sin \theta)$ from crystals of suitable lattice constants,

notably beryl (2d = 1.595 nm) and potassium acid phthalate (2.663 nm).

A summary of the work in this very interesting spectral region is given by Stratton.¹⁵

In conclusion, one can say without hesitation that most research efforts have found the medium of plasma a very elusive one and all means of extracting information concerning its properties are highly welcome. As the grosser instabilities are gradually eliminated from the confinement problem, it becomes more subtle to delineate those remaining, thereby requiring greater precision and patience on the part of the investigator.

References

- T. D. Anderson, R. W. Springer, R. C. Worder Jr, "Physico-Chemical Diagnostics of Plasmas" in Proceedings of the 5th Biennial Gas Dynamics Symposium, Northwestern University Press, Evanston, Ill. (1963).
- H. Griem, Plasma Spectroscopy, McGraw-Hill Book Co., New York (1964).
- M. A. Heald, C. B. Wharton, Plasma Diagnostics with Microwaves, John Wiley and Sons, New York (1965).
- R. H. Huddlestone, S. L. Leonard, Plasma Diagnostic Techniques, Academic Press, New York (1965).
- V. D. Rusanov, Modern Plasma Research Methods (trans. from Russian), AEC-tr-6348, U.S. Atomic Energy Commission, Washington (1964).
- B. P. Konstantinov, Plasma Diagnostics (trans. from Russian), AEC-tr-6518, US Atomic Energy Commission, Washington (1964).
- T. H. Stix, The Theory of Plasma Waves, McGraw-Hill Book Co., New York (1962).
- 8. S. C. Brown in Proceedings of the 2nd International Conference on Peaceful Uses of Atomic Energy 32, 394, United Nations, Geneva (1958).
- 9. D. Bohm, in Characteristics of Electrical Discharges in Magnetic Fields, chap. 3, (A. Guthrie and R. K. Wakerling, eds.), McGraw-Hill Book Co., New York (1949).
- K. Bol, K. Prelec, Princeton Plasma Physics Laboratory Rpt. MATT-402 (1965).
- 11. Reference 4, chap. 12.
- 12. Refence 4, chap. 3.
- R. W. P. McWhirter, W. G. Griffin,
 T. J. L. Jones in Proceedings of the 4th International Conference on Ionization Phenomena in Gases, (Uppsala, 1959), 2, 833, North-Holland, Amsterdam (1960).
- L. Heroux, Proc. Phys. Soc. (London) 83, 121 (1964).
- 15. Reference 4, chap. 8.